

Multiple Reflections and Diffuse Scattering in Bragg Scattering at Optical Lattices

S. Slama, C. von Cube, M. Kohler, C. Zimmermann, and Ph.W. Courteille

Physikalisches Institut, Eberhard-Karls-Universität Tübingen,

Auf der Morgenstelle 14, D-72076 Tübingen, Germany

(Dated: July 24, 2018)

We study Bragg scattering at 1D atomic lattices. Cold atoms are confined by optical dipole forces at the antinodes of a standing wave generated inside a laser-driven cavity. The atoms arrange themselves into an array of lens-shaped layers located at the antinodes of the standing wave. Light incident on this array at a well-defined angle is partially Bragg-reflected. We measure reflectivities as high as 30%. In contrast to a previous experiment devoted to the thin grating limit [S. Slama, *et al.*, Phys. Rev. Lett. **94**, 193901 (2005)] we now investigate the thick grating limit characterized by multiple reflections of the light beam between the atomic layers. In principle multiple reflections give rise to a photonic stop band, which manifests itself in the Bragg diffraction spectra as asymmetries and minima due to destructive interference between different reflection paths. We show that close to resonance however disorder favors diffuse scattering, hinders coherent multiple scattering and impedes the characteristic suppression of spontaneous emission inside a photonic band gap.

PACS numbers: 42.50.Vk, 42.55.-f, 42.60.Lh, 34.50.-s

I. INTRODUCTION

The idea of realizing photonic band gaps (PBG) in optical lattices, i.e. periodic arrays of cold atomic clouds confined inside standing light waves, has been published in 1995 by Deutsch *et al.* [1]. A first step towards an experimental observation of this phenomenon was made by showing that lattices of atomic gases can give rise to Bragg scattering in the very same way as X-rays are scattered in structure analyses of solid crystals [2] or molecules [3]. This demonstration has been given by G. Birkl *et al.* and M. Weidemüller *et al.* [4, 5] using near-resonant optical lattices.

In resonant lattices the optical trapping potential provides an efficient cooling mechanism for the atomic cloud. This cooling is important, because it balances heating due to inelastic scattering processes, which destroy the periodic order and decrease the Bragg scattering efficiency. Cooling is absent in conservative optical lattices tuned far from atomic resonances. On the other hand, conservative lattice potentials are interesting in view of their perspectives to mimic solid state physics. For example, Mott insulator phase transitions in degenerate atomic quantum gases have been observed [6], and fermionic gases confined in optical lattices are expected to exhibit novel quantum phases involving high-temperature superfluidity. Those phases may constitute useful toy models for superconductivity in high- T_c cuprates [7]. Bragg diffraction could represent a novel and powerful tool for sensitively probing the properties of such optical crystals provided the destructive influence of resonant probe light absorption is mastered.

PBGs are today extensively studied in crystals and fibers. Dielectric materials offer the possibility of realizing complex periodic structures in three dimensions alternating high and low index of refraction domains. Those structures, called photonic crystals, can exhibit ranges of frequencies known as photonic band gaps for which the

propagation of electromagnetic waves is classically forbidden in certain directions [8]. Tailoring of the density of states for the electromagnetic modes allows for controlling fundamental atom-radiation interactions in solid state environments and even to suppress vacuum fluctuations. The hallmarks of a PBG are the inhibition of spontaneous emission, an effect that has been observed with optical cavities [9] and the possibility of Anderson localization of light by point defects added to the photonic band gap material.

Although impressive progress has been made [10] in fabricating photonic crystals, they suffer from fundamental difficulties in guaranteeing the required fidelity over long ranges [11] due to fluctuations in position and size of the building blocks. This disorder perturbs those properties of photonic crystals based on global interference: It reduces the Bragg reflectivity, extinguishes the transmitted light, and ultimately destroys the photonic band gap. On the other hand, optical lattices exhibit an intrinsically perfect periodicity. Local disorder introduced by thermal fluctuations in the atomic density distribution at each lattice site reduces the value of the Debye-Waller factor [12], but does not affect the quality of the long-range order.

To observe photonic band gaps with optical lattices, one must reach the *thick grating regime*. However, all Bragg scattering experiments on optical lattices have so far [4, 5, 13] been performed in the *thin grating regime*, where the lattice's optical density is so low that multiple light scattering events are rare. Bragg scattering at thin lattices is understood as resulting from constructive interference of the Rayleigh-scattered radiation pattern emitted by periodically arranged point-like sources. In this regime, the reflection coefficient of the lattice turns out to be nearly real, phase shifts are negligible, and spectral lineshapes are symmetric. In particular, since the scattering takes place as a local process, which means that the light is scattered by individual atoms, the *atomic*

positions do not shape the absorption spectrum [14].

In contrast, the thick grating regime is characterized by multiple reflections of the incident light between the stacked atomic layers (Bragg planes). The interference between the light reflected from or transmitted through the layers gives rise to stopping bands for certain light frequencies or irradiation angles. In this regime, absorption can generally be neglected, but large phase shifts occur, and the lineshapes are asymmetric. Multiple beam interference globalizes the scattering process.

In this work we study a one-dimensional optical lattice consisting of a standing light wave filled with trapped atoms. The atoms arrange themselves into a linear array of lens-shaped clouds aligned along their symmetry axis. The clouds have a finite radial extent and are centered at the locations of the antinodes. We show that for this configuration the thick grating regime is within experimental reach. In fact, which regime is realized in experiment depends on the available effective number of scattering layers. The number of populated antinodes sets an upper limit. However the finite radial extent of the layers also limits the number of multiple reflections when the angle of incidence for the Bragg light is large. Therefore, to get into the thick grating regime, we have modified the setup of a previous experiment [13] in order to reduce the Bragg angle and increase the radial extent of the Bragg layers. With this setup we encounter a new limitation: When the probe laser is tuned close to an atomic resonance, detrimental absorption due to disordered atoms reduces the effective number of layers involved in multiple scattering and dominates the spectra. Off-resonance, in contrast, the weak Bragg scattering efficiency brings us into the thin grating regime. Hence, it is important to identify clear signatures of multiple scattering in optical lattices and to develop sensitive tools for their detection.

In some respects, we may understand the 1D optical lattice as a dielectric mirror with layers made of a dilute atomic gas. On the other hand, as shown in Ref. [15], the 1D optical lattice shares the peculiarities of a linear array of point-like scatterers.

Several authors [4, 12, 16] suggested optical lattices for the creation of 3D photonic band gaps. However, a consequence of the narrow width of the atomic resonance is that *Bragg scattering at gaseous lattices is intrinsically one-dimensional*. This holds also for 2D and 3D geometries of optical lattices, so that the results of our investigations apply to all kinds of lattice configurations. The low dimensionality of the scattering problem thus compromises the realization of true 3D photonic band gaps with optical lattices.

We organized this paper as follows: In section II we present our experimental setup, show examples of typical spectra, and discuss how diffuse scattering interferes with multiple reflections. To qualitatively understand the spectra a transfer matrix model is developed in section III. Based on Ref. [1] the model is extended to comply with partially disordered lattices and inhomogeneous

Stark shifts. The model provides a simple picture for the observed spectra allowing for a discrimination between diffuse and multiple scattering. It also describes the expected suppression of spontaneous emission and yields a quantitative prediction of the lattice's reflection and transmission as a function of experimental parameters. Section IV presents our observations and discusses them in terms of multiple reflections and diffuse scattering. Since both effects give rise to similar signatures in the reflection spectra, they are difficult to separate, in particular in the presence of experimental imperfections. As summarized in section V, despite the fact that some signatures strongly suggest the concurrence of multiple reflections, it seems actually beyond reach to see suppression of spontaneous emission due to a reduced density of optical states.

II. EXPERIMENT

A. Setup

The optical layout of our experiment shown in Fig. 1 is identical to the one presented in Ref. [15]. It consists of an optical cavity and a setup for Bragg scattering. The light of a titanium-sapphire laser operating at $\lambda_{\text{dip}} = 808 - 812$ nm, which is red-detuned with respect to the rubidium D_1 line, is coupled and phase-locked to the cavity. The standing wave which builds up inside the cavity has a periodicity of $\frac{1}{2}\lambda_{\text{dip}} = \pi/k_{\text{dip}}$. The beam diameter at the center of the cavity is $w_{\text{dip}} = 220$ μm . The intracavity light power is $P_{\text{cav}} = 5$ W. Between $N = 10^5$ and 10^7 ^{85}Rb atoms are loaded from a standard magneto-optical trap (MOT) into the standing wave. About 10000 antinodes are filled with atoms. Typically the temperature of the cloud is on the order of few 100 μK . In earlier experiments [15] we found that the temperature of the cloud tends to adopt a fixed ratio with the depth of the dipole trap, $k_{\text{B}}T \approx 0.4U_0$ [17]. Therefore, the spatial distribution of the atoms does not vary much with the potential depth. From this we derive the *rms*-size of an individual atomic cloud along the cavity axis, $2\sigma_z = \frac{1}{\pi}\lambda_{\text{dip}}\sqrt{k_{\text{B}}T/2U_0} \approx 115$ nm in the harmonic approximation of the trapping potential. The radial size is $2\sigma_r = w_{\text{dip}}\sqrt{k_{\text{B}}T/U_0} \approx 140$ μm and the mean density lies between $n = 3 \times 10^9$ and 3×10^{11} cm^{-3} . For the present setup we estimate a Debye-Waller factor of $f_{\text{DW}} = e^{-2k_{\text{dip}}^2\sigma_z^2} \approx 0.2$ [15].

The light used to probe the Bragg resonance is generated with a near infrared laser diode operating at $\lambda_{\text{brg}} = 780$ nm. The laser light is passed through an acousto-optic modulator (AOM) and an optical fiber and collimated to a beam waist of $w_{\text{brg}} = 800$ μm before crossing the dipole trap standing wave under an angle of $\beta_i \simeq \arccos(\lambda_{\text{brg}}/\lambda_{\text{dip}})$, which at $\lambda_{\text{dip}} = 810$ nm is about 15.6° . The incident laser power, $P_i = 30$ μW , is well below saturation. Some time after loading the atoms into the standing wave the probe beam is switched

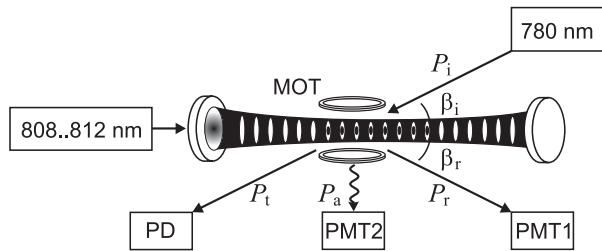


FIG. 1: The experimental setup consists of a cavity pumped with a titanium-sapphire laser at 808 - 812 nm and a diode laser at 780 nm for Bragg scattering. About 10000 antinodes of the cavity mode are loaded with ^{85}Rb atoms from a MOT. Observed are the reflected (PMT1), the transmitted (PD) and the absorbed (PMT2) light powers.

on and frequency-ramped across the rubidium D_2 resonance. The light power reflected from the atoms P_r is detected under the angle $\beta_s = -\beta_i$ with a photomultiplier (PMT1). The transmitted light power P_t is recorded with a photodiode (PD), and the isotropically scattered power P_a is detected by collecting the light emission into a solid angle of 0.05 sr orthogonal to the incident probe beam with a second photomultiplier (PMT2).

To obtain Bragg reflection the angle of incidence of the probe laser has to be matched to the lattice constant. Experimental fine tuning of the Bragg condition is however easier by varying the wavelength of the lattice laser, $\Delta\lambda_{\text{dip}} \equiv \lambda_{\text{dip}} - \lambda_{\text{brg}} / \cos \beta_i$, while the angle of incidence is kept fixed.

B. Bragg spectra

The experimentally accessible quantities are the reflected, transmitted and absorbed light powers. We take simultaneous spectra of these quantities by ramping the probe laser frequency across the Bragg resonance. In order to compare with calculations we are interested in the reflection, transmission and absorption coefficients R, T , and A . A direct comparison is complicated by the fact that the probe beam cross section is larger than the size of the atomic cloud, so that only a fraction $\eta \approx 16\%$ of the incident power P_i really overlaps with the atomic cloud [18],

$$\begin{aligned} P_r &= R\eta P_i, \\ P_t &= T\eta P_i + (1 - \eta)P_i \\ P_a &= A\eta P_i. \end{aligned} \quad (1)$$

Therefore the energy conservation requirement, $P_i = P_r + P_t + P_a$, implies $R + T + A = 1$.

Fig. 2(a) shows reflection, transmission and absorption spectra of the Bragg resonance obtained by ramping the detuning of the probe laser Δ_{brg} from the D_2 resonance. The resonance linewidth is $\Gamma/2\pi = 6$ MHz. Note the high Bragg reflection efficiency of more than 30%, which

is more than two orders of magnitude higher than in any previous measurement on optical lattices.

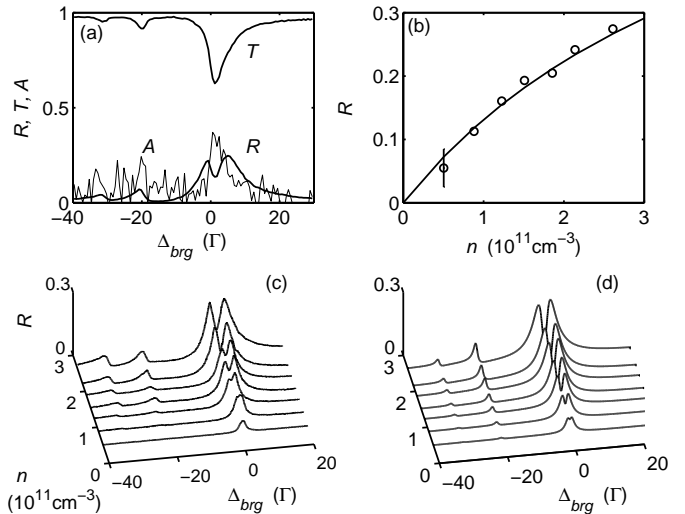


FIG. 2: (a) Reflection (lower thick trace), transmission (upper trace) and absorption spectra (noisy thin trace) of Bragg scattering. (b) Dependence of the absolute maximum of the reflection spectra on the atom number. The maximum Bragg diffraction efficiency saturates for large atom numbers. The theoretical curve assumes $N_s = 400$ scattering layers and a Debye-Waller factor of $f_{\text{DW}} = 0.2$. (c) Measured Bragg spectra for various atomic densities. The small peaks at $\Delta_{\text{brg}} = -31\Gamma$ and -20Γ corresponds to transitions from the ground state hyperfine level $F = 3$ to the excited state levels $F' = 2, 3$, the broad peak around $\Delta_{\text{brg}} = 0$ to the level $F' = 4$. For the calculations (d) the optical cross sections at the various hyperfine transitions have been weighted according to their relative oscillator strength.

The scattering efficiency for standard Bragg diffraction depends quadratically on the atom number. This dependency has been observed in Ref. [13] in the thin grating regime. The measurements performed with the present apparatus exhibit a different behavior. As seen in Fig. 2(b) at large atom densities the scattering efficiency seems to saturate. Also the shape of the reflection signal depends critically on the atom number. At very low atom number we find a Lorentzian lineshape, whose width corresponds to the natural linewidth of the D_2 line. When the atom number is increased, the linewidth broadens and the peak saturates. At large atom numbers a pronounced dip appears at the center of the strongest resonance of the reflection spectrum [4], whose contrast increases with increasing atomic density [cf. Fig. 2(c)]. Theoretical predictions based on transfer matrices calculations presented below confirm this behavior [cf. Fig. 2(d)]. The main goal of this paper is to explain these observations.

C. Specular versus diffuse scattering

The atoms are strongly localized in axial direction at the center of the antinodes. Consequently, the spectrum of the light reflected into the Bragg angle is narrowed by the Lamb-Dicke effect, and the axial thermal distribution of the atoms does not broaden the angular distribution of the reflected radiation, but increases the background of isotropically distributed diffuse scattering. This behavior is known from Bragg scattering of X-rays at solids. In contrast the weak radial confinement of the atoms does broaden the angular distribution [15].

The finite radial atomic distribution has however a more important impact on the reflected light. The radial size of the atomic cloud determines the length of the probe beam trajectory across the lattice. Thus for thick lattices, when multiple scattering plays a role, the maximum number of reflections, i.e. the effective number of layers, is limited to $N_s = 2\sigma_r / (\lambda_{\text{dip}} \tan \beta_i)$. In an earlier experiment [13] we have studied Bragg scattering at an optical lattice near the $5S_{1/2} - 6P_{3/2}$ transition at 420 nm. The corresponding Bragg angle was 58° yielding $N_s \approx 100$. In the present setup we use a linear cavity with a larger mode waist and operate the probe light near the D_2 line. This decreases the Bragg angle to 15.6° and increases the effective number of layers to $N_s \approx 600$.

At first glance, the saturation behavior observed in Fig. 2(b) could be interpreted as an indication for multiple scattering. The dips appearing in Fig. 2(c) could result from different multiple scattering trajectories of the probe laser along the lattice, which destructively interfere for certain values of the incident angle and of the probe light frequency. However, as already demonstrated in Ref. [4] the situation is more complex. In fact in a thermal lattice, for a small Debye-Waller factor, $f_{\text{DW}} \ll 1$, disordered atoms have a dramatic influence on the scattering: 1. They reduce the number of ordered atoms contributing to Bragg scattering. 2. They absorb and attenuate the incident light, and hence *decrease the penetration depth of the probe beam and thus the effective number of layers available to Bragg and in particular to multiple scattering.*

A first approach in describing the physical situation may consist in dividing the atomic cloud into two parts: a perfectly ordered optical lattice with density nf_{DW} and a homogenous cloud having the density $n(1 - f_{\text{DW}})$. The homogeneous cloud limits the penetration depth to $z_{\text{pd}} = [\sigma n(1 - f_{\text{DW}})]^{-1}$, which corresponds to a reduced effective number of layers $N_{s,\text{pd}} = 2z_{\text{pd}}/\lambda$. The effective number of layers thus critically depends on the density of disordered atoms and, via the optical cross section σ , on the detuning Δ_{brg} . On resonance assuming a density $n \approx 3 \times 10^{11} \text{ cm}^{-3}$ we estimate $N_{s,\text{pd}} \approx 37$ [19]. As a consequence, we expect a dramatic break-down of the Bragg reflection signal close to resonance, where the absorption by the unordered atoms is largest. The frequency range for absorption, being on the order of the

natural linewidth Γ , is much smaller than the width of the reflection signal, which explains the appearance of a narrow dip in the reflection spectra Fig. 2(c). In particular, *signatures of multiple scattering will not show up in parameter regimes, where the number of scattering layers is considerably reduced below N_s , $N_{s,\text{pd}} \ll N_s$.*

Note that the separation of the Bragg reflection into a perfectly ordered contribution and diffuse scattering corresponds to an ansatz frequently made in treating disorder and impurities in crystals [12, 20].

III. THEORETICAL MODELING

A. Transfer matrix formalism

In the following we attempt to provide a more quantitative understanding of the observations by developing a simple theoretical model. We start by relating the atomic polarizability α (given in SI-units) to the single-layer reflection coefficient ζ via

$$\begin{aligned} \zeta &= -n\delta z \frac{k_{\text{brg}}}{2} \frac{\alpha}{\epsilon_0} \\ &= -n\delta z \frac{3}{2} \frac{\lambda_{\text{brg}}^2}{2\pi} \frac{1}{i + 2(\Delta_{\text{brg}} - \Delta_F)/\Gamma}, \end{aligned} \quad (2)$$

where $n\delta z$ is the surface density estimated for a homogeneous atomic density n and a layer thickness δz . To account for the presence of several hyperfine transitions at frequency detunings Δ_F [cf. Fig. 2(d)], we build the weighted sum of the individual oscillator strengths.

For the description of the collective influence of the atoms on the incident light, we use a generalization of the transfer matrix formalism presented in Ref. [1]. The generalization concerns two major points: First of all, in that reference the probe beam was assumed collinear with the optical lattice beams, while in our case the angle of incidence is significantly different from 0. In fact the deviation of the chosen angle from the Bragg angle constitutes an additional degree of freedom allowing us to tune frequency and quasi-momentum independently. Again, in practice we detune the lattice constant rather than the angle of incidence. A second generalization consists in the inclusion of diffuse scattering into the formalism, as detailed in the next section. All theoretical lineshapes shown in the figures are obtained from this transfer matrix model.

We will now supply the basic ingredients of the model skipping the details already reported in Ref. [1]. The in- and outgoing field amplitudes of the probe beam at any axial location z of the lattice (the model is one-dimensional) are labeled $E^+(z)$ and $E^-(z)$, respectively. Their variation from one location to another is described by a transfer matrix M , such that (in the complex representation)

$$\begin{pmatrix} E^+(z) \\ E^-(z) \end{pmatrix} = M \begin{pmatrix} E^+(0) \\ E^-(0) \end{pmatrix}. \quad (3)$$

The procedure consists now in dividing the atomic sample into layers. The transfer matrix for interaction of the probe light with a single infinitely narrow layer of the optical lattice characterized by the surface density $n\delta z$ is

$$A_\zeta = \begin{pmatrix} 1 + i\zeta & i\zeta \\ -i\zeta & 1 - i\zeta \end{pmatrix}. \quad (4)$$

The transformation of the field amplitudes *between* two such layers separated by Δz is described by

$$B_{\Delta z} = \begin{pmatrix} e^{ik_{\text{brg}}\Delta z \cos \beta_i} & 0 \\ 0 & e^{-ik_{\text{brg}}\Delta z \cos \beta_i} \end{pmatrix}. \quad (5)$$

Hence the total transfer matrix for a lattice with N_s layers reads $M = (A_\zeta B_{\Delta z})^{N_s}$. Finally the reflection coefficient $R = |r|^2$ and the transmission coefficient $T = |t|^2$ are calculated via

$$r = \frac{M_{12}}{M_{22}}, \quad t = \frac{1}{M_{22}}, \quad (6)$$

while the phase shift in reflection follows from $\phi = \arctan(\text{Im } r / \text{Re } r)$. If we identify a layer with an antinode of the standing wave, $\Delta z = \delta z = \lambda_{\text{dip}}/2$, we obtain from the Eqs. (6) Bragg spectra for the case of a perfect lattice, such as those shown in Figs. 3(a-c).

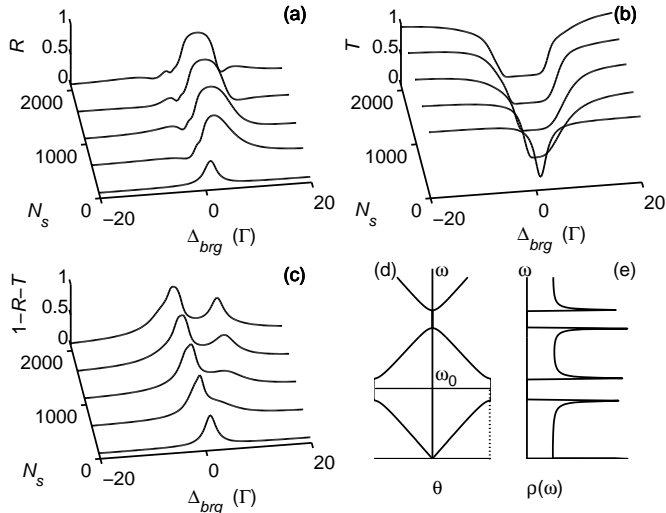


FIG. 3: The figures (a), (b), and (c) show calculated Bragg reflection, transmission and absorption spectra for lattices with various numbers of layers N_s . Here we assumed $f_{\text{DW}} = 1$ and $n = 3 \times 10^{11} \text{ cm}^{-3}$. The lattice is slightly detuned from the Bragg condition, $\Delta\lambda_{\text{dip}} = 0.8 \text{ nm}$, so that the lineshapes become asymmetric. (d) Sketch of the photonic dispersion relation. The opening of a band gap for values of the quasi-momentum θ near the edges of the Brillouin zone indicates a suppression of the density of states $\rho(\omega)$ as drawn in figure (e).

B. Sequential density model

Instead of separating the atomic cloud into a perfectly ordered lattice and a homogeneous density distribution as proposed in Sec. II C, we may subdivide every layer into a number N_{ss} of sublayers for which we evaluate the transfer matrices based on the local density,

$$n_{\text{loc}}(z) = n \frac{\lambda_{\text{dip}} e^{-U(z)/k_B T}}{2N_{\text{ss}} \int e^{-U(z')/k_B T} dz'}, \quad (7)$$

where $U(z) = -U_0 \cos k_{\text{dip}} z$ is the trapping potential, or in the harmonic approximation $U(z) = U_0 k_{\text{dip}}^2 z^2 = k_B T z^2 / 2\sigma_z^2$. Now we recalculate the local single-layer reflection coefficient ζ_{loc} as in Eq. (2) and set up the total transfer matrix, but using the *local* density $n_{\text{loc}}(z)$ instead of a homogeneous density n and setting the layer thickness to $\delta z \equiv \lambda_{\text{dip}}/2N_{\text{ss}}$,

$$M = \left(\prod_{\nu=1}^{N_{\text{ss}}} A_{\zeta_{\text{loc}}} \left(\frac{2\nu\delta z}{\lambda_{\text{dip}}} \right) B_{\delta z} \right)^{N_s}. \quad (8)$$

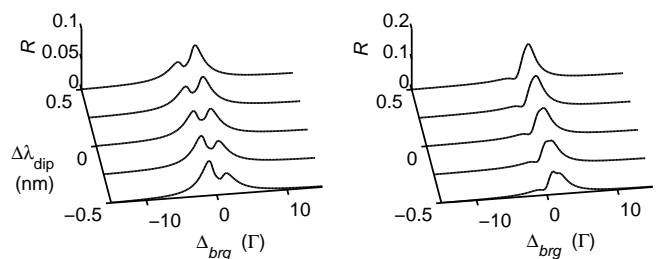


FIG. 4: Calculated Bragg reflection spectra for various detunings of the lattice constant from the Bragg condition (a) without and (b) with Stark-shift. We assumed $n = 3 \times 10^{11} \text{ cm}^{-3}$, $N_s = 200$ and $N_{\text{ss}} = 20$. At a potential depth $U_0 = 500 \mu\text{K}$ we assume $k_B T \approx 0.4U_0$.

At finite temperatures the atoms are distributed over the optical potential and thus experience individual dynamical Stark shifts of their resonances varying with the atoms' locations. This leads to serious inhomogeneous broadening of the Bragg spectra as shown in Ref. [13]. Cold atoms which concentrate at the antinodes of the standing wave potential are Stark-shifted by a large amount and form the blue edge of the line profile. The hot part of the cloud sees on average a shallower potential and forms the red tail of the profile. A possible approach to describe the line broadening consists in building the convolution of the spectra calculated from Eqs. (6) and (8) with the probability density of finding an atom at a given potential energy. However this approach does not account for the fact that in the thick grating limit cold (predominantly ordered) and hot (mostly disordered) atoms yield qualitatively different lineshapes of the Bragg reflection signal. In other

words, the convolution procedure is incompatible with the fact that the contributions of cold and hot atoms to the Bragg-scattered light depends on the penetration depth, which itself varies with the frequency detuning of the probe beam.

Fortunately, the local Stark shift is easily included in the sequential densities model via the substitution

$$\Delta_{\text{brg}} \rightarrow \Delta_{\text{brg}} - U(z). \quad (9)$$

The figures 4(a,b) show calculated reflection spectra without and with Stark shifts for various detunings of the lattice constant from the Bragg condition. As in Figs. 2(b,c) the dip in the spectra corresponds to a joint impact of diffuse and multiple scattering and will be discussed in more detail in Sec. IV A. Here we just point out that Stark broadening obviously induces pronounced asymmetries with respect to $\Delta\lambda_{\text{dip}}$.

We verified that in the limit of a perfect lattice, obtained for $T \rightarrow 0$, the line broadening disappears. The lines are just blue-shifted by an amount U_0/\hbar . In the thin grating regime, obtained for small densities $n < 10^{11} \text{ cm}^{-3}$, the convolution approach and the sequential densities approach yield identical spectra.

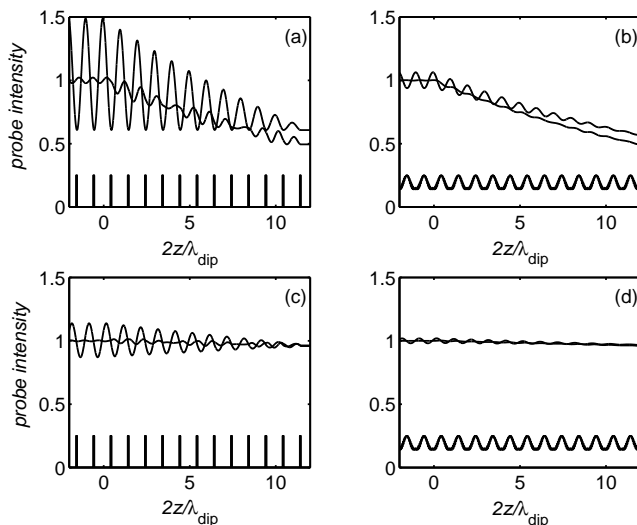


FIG. 5: **(a)** Evolution of the light intensity across the optical lattice normalized to the incident probe beam intensity for $\Delta\lambda_{\text{dip}} = 0$ (large amplitude oscillations) and $\Delta\lambda_{\text{dip}} = 200 \text{ nm}$ (small amplitude oscillations). The last detuning has been chosen to be extreme in order to visualize the rapid decay of the intensity even for a low number of layers $N_s = 10$. The probe was tuned to resonance, $\Delta_{\text{brg}} = 0$. The spikes at the bottom of the pictures indicate the maxima of the atomic density distribution assumed to describe a perfect lattice, $f_{\text{DW}} = 1$. **(b)** Same as (a) but with $f_{\text{DW}} \simeq 0.03$. The lowest curve shows the axial atomic density distribution. **(c,d)** Same as (a) and (b) respectively, but now the probe laser has been detuned to $\Delta_{\text{brg}} = \Gamma$.

C. Suppression of absorption

The hallmark of 3D photonic crystals is the suppression of spontaneous emission. The models describing the propagation of light inside photonic crystals assign this suppression to a reduction of the density of optical modes available for spontaneous decay [8]. In fact the frequency dependence of the density of states, sketched in Fig. 3(e), is characterized by forbidden bands. As pointed out in Ref. [1], 1D optical lattices exhibit similar band gaps. This can be seen in Fig. 3(a-c). For large numbers of scattering layers, $N_s \gtrsim 1000$, the lattice gets opaque. The transmission vanishes over a large range of frequency detunings Δ_{brg} , while the reflection is close to unity. Even more interesting is the feature that the absorption spectrum $1 - R - T$ splits into two peaks, and the absorption vanishes in the center of the band gap.

At first glance this may seem surprising. Since the geometry of our lattice is 1D, we would not expect a noticeable modification of the density of decay modes. This is similar to the inhibition of spontaneous emission inside linear optical cavities [9]: An excited atom may decay into all the transverse modes leading out of the cavity. If the cavity only covers a small solid angle of the radiating atom, its spontaneous decay rate will only be reduced by a small amount.

The reduction of the absorption inside a band gap of an optical lattice has a different origin. A deeper understanding of the system is gained by calculating the progression of the probe light intensity along the optical lattice using the above transfer matrix formalism under various conditions (cf. Fig. 5). First of all, we find that the standing wave formed by the incident probe beam and the Bragg-reflected light adjusts its phase such that its *nodes coincide with the atomic layers*. In that way absorption is minimized. If the length of the lattice is finite, the contrast of the standing wave is smaller than 1, i.e. the probe light intensity at the locations of the atomic layers does not vanish. Hence a finite absorption subsists even, when the lattice is perfect and the Bragg condition fulfilled.

Let us now study the response of the probe standing wave to variations of experimental parameters. Fig. 5(a) compares the cases of an aligned and a misaligned angle of incidence with respect to the Bragg angle. For a misaligned angle the periodicity of the probe standing wave does not coincide with the lattice constant, which results in a displacement of the nodes from the atomic layers and hence in enhanced absorption. The contrast of the probe wave is smaller than for an aligned angle. However, as the probe light penetrates deeper into the lattice, the displacement gets smaller and the probe wave contrast adopts the value of the aligned case.

The curves shown in Fig. 5(a) assume a perfectly ordered lattice. In the presence of disordered atoms, i.e. atoms which are not confined to the locations of the probe beam intensity minima, absorption can take place anywhere. We thus obtain an additional background of

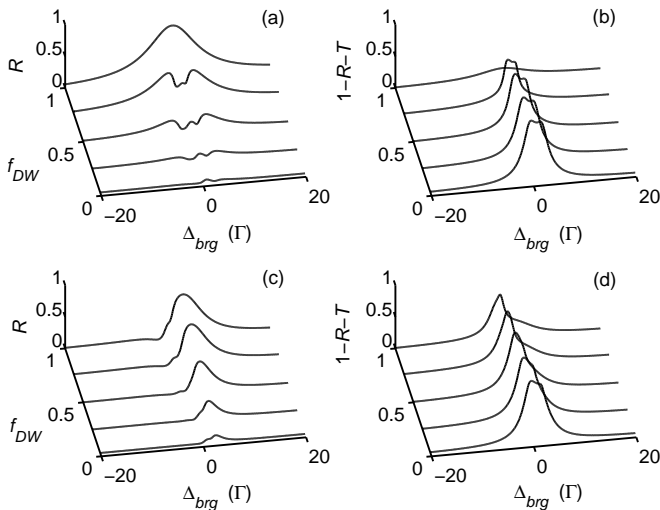


FIG. 6: Reflection (a) and absorption spectra (b), calculated for various values of the Debye-Waller factor f_{DW} . The other parameters are $\Delta\lambda_{dip} = 0$, $n = 3 \times 10^{11} \text{ cm}^{-3}$, and $N_s = 600$. (c,d) Same as (a) and (b), but with $\Delta\lambda_{dip} = 0.8 \text{ nm}$.

absorption, which in the extreme case of strong disorder leads to a fast exponential decay according to the Lambert-Beer law. The exponential curves in Fig. 5(b) are obtained under the same conditions as in (a), but with a finite Debye-Waller factor, $f_{DW} = 0.03$. Finally when the probe beam is tuned off resonance, the absorption is smaller and the penetration depth is drastically increased. This is shown in Figs. 5(c-d), which corresponds to (a-b) respectively, but with a probe laser detuning set to $\Delta_{brg} = \Gamma$.

In summary, absorption occurs for two reasons: Either the Bragg angle is mismatched, or the atoms are disordered. This is illustrated by calculations of reflection and absorption spectra shown in Fig. 6. For example, the spectrum in Fig. 6(d) corresponding to $f_{DW} = 1$ shows an absorption peak despite perfect atomic ordering, because the Bragg angle is not matched; and the spectra in Fig. 6(b) corresponding to $f_{DW} < 1$ show finite absorption although the Bragg angle is matched. Reduced absorption is only observed for a perfect lattice *and* a matched angle of incidence for the probe beam [see curve corresponding to $f_{DW} = 1$ in Fig. 6(b)].

IV. OBSERVATIONS

A. Signatures of multiple scattering

The appearance of signatures for multiple scattering depends very much on the available effective numbers of layers. As we have seen in Sec. II C diffuse scattering drastically reduces the number of layers from $N_s = 600$ to $N_{s,pd} = 37$, which is clearly insufficient to produce dips

in the reflection spectrum corresponding to destructive interference of different reflection paths. Fig. 3(a) reveals that for our atomic densities several hundred layers are necessary to significantly distort the spectrum near the photonic band edge.

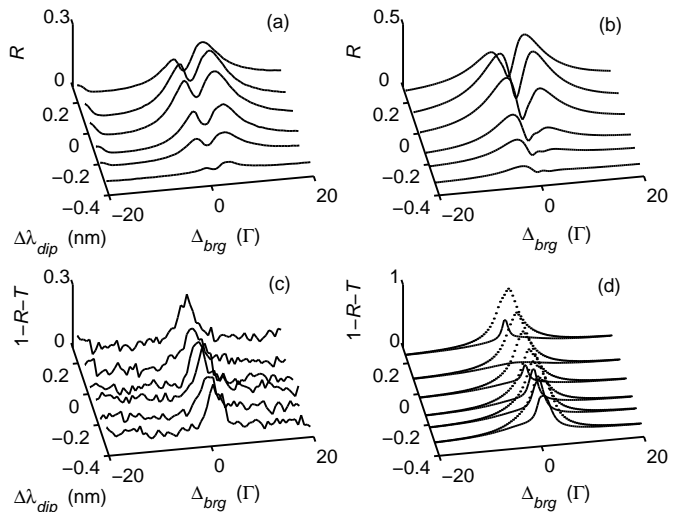


FIG. 7: Measured (a) and calculated (b) Bragg reflection spectra for various dipole laser frequencies. Measured (c) and calculated (d) absorption. The calculations are based on $n = 3 \times 10^{11} \text{ cm}^{-3}$, $N_s = 200$, and $f_{DW} = 0.7$ (dotted lines) and $f_{DW} = 1$ (solid lines).

In order to observe signatures of a band edge, the angle of incidence of the probe beam must be chosen in such a way that they appear outside the detuning range, where diffuse scattering is dominant. In fact already at $|\Delta_{brg}| > 3\Gamma$ the penetration depth allows for an effective number of layers larger than 600.

Fig. 7(a) shows Bragg reflection spectra measured for various lattice constants. Fig. 7(c) shows simultaneously recorded absorption spectra. Figs. 7(b,d) represent corresponding calculations. Although the reflection spectra are in qualitative agreement, there is a striking difference. While for the measured spectra the dip is always close to the line center, the symmetry of the calculated spectra changes when going from negative to positive $\Delta\lambda_{dip}$. An explanation for this is given in Sec. IV B.

The amount of absorption measured in the experiment does not depend much on λ_{dip} . This is confirmed by the simulations [dotted lines in Fig. 7(d)]. The reason for this is diffuse scattering due to atomic disorder as discussed in Sec. III C [21, 22]. For comparison we have also plotted in Fig. 7(d) the spectra calculated for zero temperature (solid lines). The effect of absorption reduction expected for $f_{DW} = 1$ is not observed in experiment.

Fig. 8(a) shows a set of spectra recorded for various atomic densities. Fig. 8(b) shows the corresponding calculations. The spectra exhibit a well-developed splitting of the dip structure. This splitting can not be explained by diffuse scattering alone, which means that multiple

reflections must play a role.

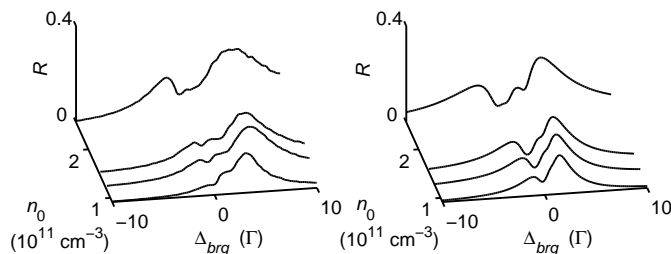


FIG. 8: Occurrence of double dips in the reflection spectra. Measurements are shown in (a). The calculations (b) assume $\Delta\lambda_{\text{dip}} = 0.08$ nm, $n = 3 \times 10^{11} \text{ cm}^{-3}$, $N_s = 520$, $U_0 = 0.6\Gamma$, and $T = 90 \mu\text{K}$.

The number of free parameters is large, therefore it is difficult to pin down the precise value of the experimental parameters by fitting. However, there is no realistic parameter regime for which our theoretical model predicts splittings of the dip without the assumption of multiple scattering. Hence, we consider the double dip feature of Fig. 8 as the first indication for the existence of a $1D$ photonic band gap in an optical lattice.

B. Experimental side effects

Various experimental deficiencies can make the quantitative interpretation of the spectra difficult. First of all, when the probe laser is detuned from resonance, its light will be bent by refraction when it enters the optically thick cloud of atoms. On one hand, this slightly modifies the angle of incidence and thus its deviation from the Bragg angle. Since this deviation depends on the probe beam detuning, the parameters $\Delta\lambda_{\text{dip}}$ and Δ_{brg} are intertwined in a complicated way. We have measured the reflection angle as a function of Δ_{brg} and found variations up to 0.1° , which corresponds to $\Delta\lambda_{\text{dip}} = 0.4$ nm. Additionally, the optically thick cloud focuses or defocuses the incident beam depending on its detuning [23].

A second important issue is the impact of the finite radial extent of the atomic layers on the reflection angle. In Ref. [15] we have shown that, although the lattice consists of a stack of two-dimensional traps with an aspect ratio smaller than $\sigma_z/\sigma_r \approx 10^{-3}$, with respect to Bragg scattering it behaves more like a chain of point-like scatterers, than like a dielectric mirror. Thus the reflection angle is not equal to the angle of incidence, but adjusts itself in order to fulfill the Bragg condition. This self-adjustment of the Bragg condition impedes a controlled tuning of $\Delta\lambda_{\text{dip}}$ and explains, why the symmetry of the traces in Fig. 7(a) does not change when the lattice constant is varied.

Furthermore, the transfer matrix model is purely one-dimensional. It assumes not only radially infinite atomic layers, but also a homogeneous density distribution. In

reality the radial density distribution is rather Gaussian, which implies a variation of the penetration depth with the distance from the optical axis. The observed reflection spectra thus represent an average of reflection spectra taken for different optical densities.

Finally, optical pumping between the ground state hyperfine levels and heating due to resonant absorption may occur while scanning the probe beam frequency and distort the spectra. These effects can however be accounted for in a simple rate equation model, which yields very good agreement with our observations.

V. DISCUSSION AND CONCLUSION

The observations made with our apparatus clearly show features beyond Bragg scattering. These are due to two effects: Disorder arising from the thermal distribution of the atoms introduces strong absorption close to resonance, which limits the effective number of layers. The second effect is multiple scattering between adjacent layers. Even though the above effects tend to distort or broaden the features, which are characteristic for multiple scattering, we find unambiguous signatures of multiple reflections. At this stage, it is however difficult to exactly quantify the number of layers involved in multiple scattering. In any case, for our present parameters the absorption spectra do not show any significant reduction at resonance, so that the qualification of *photonic band gap* seems not adequate.

An interesting question concerns the signature of atomic ordering in the transmitted and the absorbed light. In the thin grating regime, one would not expect that the atomic positions influence the absorption: the behavior of an absorbing atom does not depend on the location of the other atoms. Moreover, unlike for the reflection signal, interference plays no role in forward scattering nor in diffuse scattering. Hence there is no signature of atomic ordering in T and A . The situation completely changes in the thick grating regime, where multiple scattering between subsequent atomic layers leads to interference between the light reflected from or transmitted through the layers. The globalization of the scattering process leads to interatomic correlation: Now it matters how the atoms are arranged. Multiple reflections give rise to stopping band gaps for certain ranges of light detuning or angle of incidence. It might therefore be more unambiguous to look for signatures of photonic band gaps in transmission or absorption spectra.

To conclude we have shown that long-range spatial order in atomic clouds can have a dramatic influence on the scattering of light. We have extended earlier studies on Bragg scattering into the regime of thick gratings characterized by multiple reflections. Although signatures for reduced absorption could not be found due to the fatal influence of diffuse scattering, this represents a first step towards the realization of photonic band structures in

optical lattices.

Differently from photonic crystals or solid state systems, the scattering off optical lattices is weak except near atomic resonances. Therefore photonic stopping bands are expected to be very narrow. This bears the advantage that we can tune the optical density over a large range. However, the narrow resonance also implies that our system is intrinsically one-dimensional. An extrapolation to three-dimensional systems seems technically demanding, first of all because 3D optical lattices have low filling factors of typically 0.01. There are however examples of lattices with unity filling factor [24]. Bose-condensates in the Mott insulator phase may prove useful to guarantee a high and regular occupation of the lattice sites [6]. On the other hand, the sharpness of the resonance results in a very narrow tolerance angle for the stop band, which will make it difficult to obtain 3D PBGs. Coevorden *et al.* [16] did numerical calculations of the band structure of a 3D optical lattice. To obtain a 3D PBG around an atomic transition of frequency ω ,

they had to assume an excessively large spontaneous decay width, $\Gamma > 0.01\omega$.

A major advantage of using *ultracold* atoms would be the total absence of diffuse scattering. Other possible technical upgrades include the use of standing waves with larger beam waists, thus extending the radial size of the atomic layers, and the choice of smaller Bragg angles, which could be done by operating the dipole trap a few nm red-detuned from the same transition, the probe laser is tuned to. Thus, although it seems today difficult to compete with photonic crystals in terms of manipulating the propagation of light just by choosing a smart arrangement of gaseous atoms, there is much room left for improvements.

We acknowledge financial support from the Landesstiftung Baden-Württemberg.

-
- [1] I. H. Deutsch, R. J. C. Spreeuw, S. L. Rolston, and W. D. Phillips, *Phys. Rev. A* **52**, 1394 (1995).
- [2] E. O. Wollan, *Rev. Mod. Phys.* **4**, 206 (1932).
- [3] J. Doucand and J. P. Benoit, *Nature* **325** 644, (1987).
- [4] G. Birkl, M. Gatzke, I. H. Deutsch, S. L. Rolston, and W. D. Phillips, *Phys. Rev. Lett.* **75**, 2823 (1995).
- [5] M. Weidemüller, A. Hemmerich, A. Görlitz, T. Esslinger, and Th. W. Hänsch, *Phys. Rev. Lett.* **75**, 4583 (1995).
- [6] M. Greiner *et al.*, *Nature* **415**, 39 (2002).
- [7] W. Hofstetter, J. I. Cirac, P. Zoller, E. Demler, and M. D. Lukin, *Phys. Rev. Lett.* **89**, 220407 (2002).
- [8] S. John and M. J. Stephen, *Phys. Rev. B* **28**, 6358 (1983).
- [9] D. J. Heinzen, J. J. Childs, J. E. Thomas, and M. S. Feld, *Phys. Rev. Lett.* **58**, 1320 (1987).
- [10] M. Woldeyohannes and S. John, *J. Opt. B* **5**, R43 (2003).
- [11] A. F. Koenderink and W. L. Vos, *Phys. Rev. Lett.* **91**, 213902 (2003).
- [12] M. Weidemüller, A. Görlitz, Th. W. Hänsch, and A. Hemmerich, *Phys. Rev. A* **58**, 4647 (1998).
- [13] S. Slama, *et al.*, *Phys. Rev. Lett.* **94**, 193901 (2005).
- [14] This holds for not too high densities, where collective effects like superradiance can be disregarded.
- [15] S. Slama *et al.* *Phys. Rev. A* (R) (2005) accepted.
- [16] D. V. van Coevorden, R. Sprik, A. Tip, and A. Lagendijk, *Phys. Rev. Lett.* **77**, 2412 (1996).
- [17] In a previous experimental setup [13] the ratio was found to be $k_B T \approx 0.4U_0$ corresponding to a Debye-Waller factor of $f_{DW} \approx 0.67$.
- [18] The factor η also accounts for the lattice being longer than the effective number of layers N_s , estimated below.
- [19] This is more problematic for the D_2 line than for the 421 nm transition [12], because of the larger oscillator strength of the D_2 line, which explains that we did not observe diffuse scattering in the experiment reported in Ref. [13].
- [20] J. M. Coley: *Diffraction Physics*, North-Holland Personal Library (1995).
- [21] The disappearance of absorption corresponds to a suppression of spontaneous Rayleigh and Raman scattering.
- [22] This is somewhat in contrast to the interpretation in Ref. [4] where a cooperation between the axial Debye-Waller factor, transversal density fluctuations and a finite penetration depth were made responsible for the increase of diffuse scattering. Note that their 3D lattice had a low filling factor, and thus the surface density was smaller than 0.05 cm^{-2} while in our case it is typically 0.5 cm^{-2} .
- [23] Here it is worth mentioning the importance of a well collimated probe beam. A divergent probe beam may be expanded into several plane waves each one having a slightly different angle of incidence. Knowing that $\Delta\beta_i = 0.02^\circ$ already produces an important modification of the spectrum, the divergence should be smaller than that.
- [24] M. T. DePue, C. McCormick, S. L. Winoto, S. Oliver, and D. S. Weiss, *Phys. Rev. Lett.* **82**, 2262 (1999).

